FULL PAPER

Multitargeted-Nanoparticles

ADVANCED
HEALTHCARE
MATERIALS

www.advhealthmat.de

Multitargeted Nanoparticles Deliver Synergistic Drugs across the Blood–Brain Barrier to Brain Metastases of Triple Negative Breast Cancer Cells and Tumor-Associated Macrophages

Tian Zhang, Hoyin Lip, Chunsheng He, Ping Cai, Zhigao Wang, Jeffrey T. Henderson, Andrew M. Rauth, and Xiao Yu Wu*

Patients with brain metastases of triple negative breast cancer (TNBC) have a poor prognosis owing to the lack of targeted therapies, the aggressive nature of TNBC, and the presence of the blood–brain barrier (BBB) that blocks penetration of most drugs. Additionally, infiltration of tumor-associated macrophages (TAMs) promotes tumor progression. Here, a terpolymer-lipid hybrid nanoparticle (TPLN) system is designed with multiple targeting moieties to first undergo synchronized BBB crossing and then actively target TNBC cells and TAMs in microlesions of brain metastases. In vitro and in vivo studies demonstrate that covalently bound polysorbate 80 in the terpolymer enables the low-density lipoprotein receptor-mediated BBB crossing and TAM-targetability of the TPLN. Conjugation of cyclic internalizing peptide (iRGD) enhances cellular uptake, cytotoxicity, and drug delivery to brain metastases of integrin-overexpressing TNBC cells. iRGD-TPLN with coloaded doxorubicin (DOX) and mitomycin C (MMC) (iRGD-DMTPLN) exhibits higher efficacy in reducing metastatic burden and TAMs than nontargeted DMTPLN or a free DOX/MMC combination. iRGD-DMTPLN treatment reduces metastatic burden by 6-fold and 19-fold and increases host median survival by 1.3-fold and 1.6-fold compared to DMTPLN or free DOX/MMC treatments, respectively. These findings suggest that iRGD-DMTPLN is a promising multitargeted drug delivery system for the treatment of integrin-overexpressing brain metastases of TNBC.

1. Introduction

Triple negative breast cancer (TNBC) is a highly aggressive subtype that accounts for 15–20% of human breast cancers.[1]

T. Zhang, H. Lip, Dr. C. He, Dr. P. Cai, Z. Wang, Prof. J. T. Henderson, Prof. X. Y. Wu
Advanced Pharmaceutics and Drug Delivery Laboratory
Leslie Dan Faculty of Pharmacy
University of Toronto
144 College Street, Toronto, Ontario M5S 3M2, Canada
E-mail: xywu@phm.utoronto.ca
Prof. A. M. Rauth
Departments of Medical Biophysics and Radiation Oncology
University of Toronto
610 University Ave, Toronto, Ontario M5G 2M9, Canada

The ORCID identification number(s) for the author(s) of this article can be found under https://doi.org/10.1002/adhm.201900543.

Owing to the low expression of estrogen receptor, progesterone receptor, and human epidermal growth factor receptor 2 (HER2), endocrine and anti-HER2 therapies are ineffective against TNBC. Thus currently, standard adjuvant and neoadjuvant treatments of TNBC are limited to conventional anthracycline-taxane-based chemotherapy.[1] Despite the initial response to chemotherapy, TNBC patients have a high risk of relapse and distal metastases, especially to the brain, leading to shortened survival times.[2] A number of targeted therapies have been investigated to treat TNBC including poly(ADP-ribose) polymerase (PARP) inhibitors, immune checkpoint inhibitors, antiandrogen agents, phosphoinositide 3-kinase inhibitors, mitogen-activated protein kinase inhibitors, antiangiogenic antibody, and integrin inhibitors.[1,3]

Upregulation of cell surface $\alpha v\beta 3$ and $\alpha v\beta 5$ integrins in aggressive TNBC, especially in brain metastases and tumor-associated vasculature, has presented an opportunity for targeted therapy of TNBC using integrin-targeted peptides.[4] Of various peptide-based inhibitors of αv integrins, Cilengitide, an Arg-Gly-Asp (RGD) peptide mimetic, with high selectivity against integrins $\alpha v\beta 3$ and $\alpha v\beta 5$, reached phase 3 clinical trial; however, the results were negative.[5] This disappointing outcome may be caused by insufficient amounts of inhibitor reaching tumor cells to generate a direct cytotoxic effect against $\alpha v\beta 3$ and $\alpha v\beta 5$ positive cancer cells due to the short half-life of Cilengitide in vivo.[5] Nonetheless, RGD-conjugated nanoparticulate drug delivery systems have shown an ability to target chemotherapeutic drugs to integrin-overexpressing tumor vasculature and cancer cells.[6]

Despite the promising results in preclinical models, it is challenging to find an optimal RGD particle coverage to balance tumor accumulation against liver uptake. For example, our previous studies on cyclic RGDfK (Arg-Gly-Asp-D-Phe-Lys; cRGD) peptide-conjugated solid-lipid nanoparticles (SLN) or polymer-lipid hybrid nanoparticles (PLN) revealed that a high density of cRGD on the surface led to increased liver uptake

and vascular retention of the nanoparticles (NPs) in primary TNBC.[7] For the treatment of lung mestastases, the physiology of normal blood circulation allows for intravenously injected cRGD-PLN to first pass through the lungs, resulting in effective nanoparticle targeting to both $\alpha v\beta 3$-overexpressing cancer cells and tumor neovasculature. With a modest surface density of cRGD and co-loaded synergistic doxorubicin (DOX or D) and mitomycin C (MMC or M), the optimized RGD-DM-PLN significantly improved the treatment of lung metastases of TNBC in a mouse model as compared to nontargeted DM-PLN.[8] However, for targeting tumors that require deeper particle penetration, a cyclic nine amino acid internalizing peptide (iRGD, CRGDK/RGPD/EC) would be more appropriate because of its reported capability of improved tumor tissue and vasculature penetration compared to other types of RGD peptides.[6c,9] The penetration capability of iRGD stems from the initial binding of the peptide to αv integrins and subsequent exposure of the CendR motif which binds to neuropilin-1 receptor on endothelial cells and tumor cells, triggering tumor vasculature and tissue penetration.[9]

In addition to targeting cancer cells, increasing evidence suggests that targeting stromal cells in the tumor microenvironment (TME) would be of therapeutic significance due to their important role in promoting cancer progression.[10] Of various types of stromal cells, tumor-associated macrophages (TAMs) are the most abundant cell type in the metastatic microenvironments, including brain metastases.[11] In breast cancer, high TAM density is associated with poor patient prognosis and low efficacy of chemotherapeutic drugs and anticancer immune-modulating agents.[11c,12] Therefore, inhibition or re-polarization of TAMs by targeting their surface receptors with small molecule inhibitors, monoclonal antibodies, or drug-encapsulated nanoparticles has shown therapeutic benefit in both pre-clinical and clinical studies.[13] Recently, nanoparticle systems have been exploited to deliver cytotoxic or inhibitory drugs to cancer cells and TAMs, or to modulate TME and re-educate TAMs for enhancing chemotherapy, with promising anticancer efficacy in vivo.[14] Conceivably, targeted drug delivery to both the TAM and cancer cell populations in the metastatic microenvironment could potentially improve the treatment of brain metastasis of TNBC.

However, delivering effetive amounts of therapeutic agents to brain metastases of breast cancer is particularly difficult due to the presence of the blood-brain barrier (BBB), which is nearly intact in micrometastases with diameters less than 0.5 mm.[15] Additionally, the presence of drug efflux transporters, overexpressed on endothelial cells of brain blood microvessels, can hinder drug transport from the blood to the brain parenchyma as many anticancer drugs are known to be efficient substrates of efflux transporters.[16] Therefore, the BBB must be overcome first to deliver a drug to TAMs and cancer cells in brain metastases.

Previously we developed a terpolymer-lipid nanoparticle (TPLN) system, based on the terpolymer, poly(methacrylic acid)-polysorbate 80-grafted starch (PMAA-PS 80-g-St), that is able to facilitate BBB-crossing and deliver brain-impermeable imaging and chemotherapeutic agents to brain metastases of breast cancer in mouse models.[17] The PS 80-containing nanoparticles can recruit apolipoprotein E (ApoE) from the blood circulation and then extravasate the brain blood microvessels via low

density lipoprotein receptor (LDLR)-mediated transcytosis.[17,18] Exploiting this unique property of the terpolymer, herein, we designed an iRGD peptide functionalized TPLN co-loaded with DOX and MMC (iRGD-DMTPLN) to first cross the BBB via in situ recruited ApoE on particle surface, and then target both αv integrin-overexpressing TNBC cells by iRGD and LDLR-overexpressing TAMs (**Figure 1**).[9,19] The combination of DOX and MMC was selected because of their strong anticancer synergy when delivered simultaneously by the same nanocarrier, which was found in our previous work in multiple breast cancer cell lines including TNBC cells and corresponding mouse tumor models.[8,20] The synergism was attributable to the enhanced topoisomerase poisoning by DOX resulted from the activated DNA repair activities from the direct DNA damage by MMC as well as the increased intracellular DOX bioavailability due to reduced level of detoxifying glutathione through the bioreductive activation of MMC.[8c,21] The nanoparticle encapsulation of the two drugs synchronized their spatiotemporal co-delivery into the tumor cells at synergistic ratios, enabling their synergistic interactions which require the close proximity of the drugs within the cells.[20b,21]
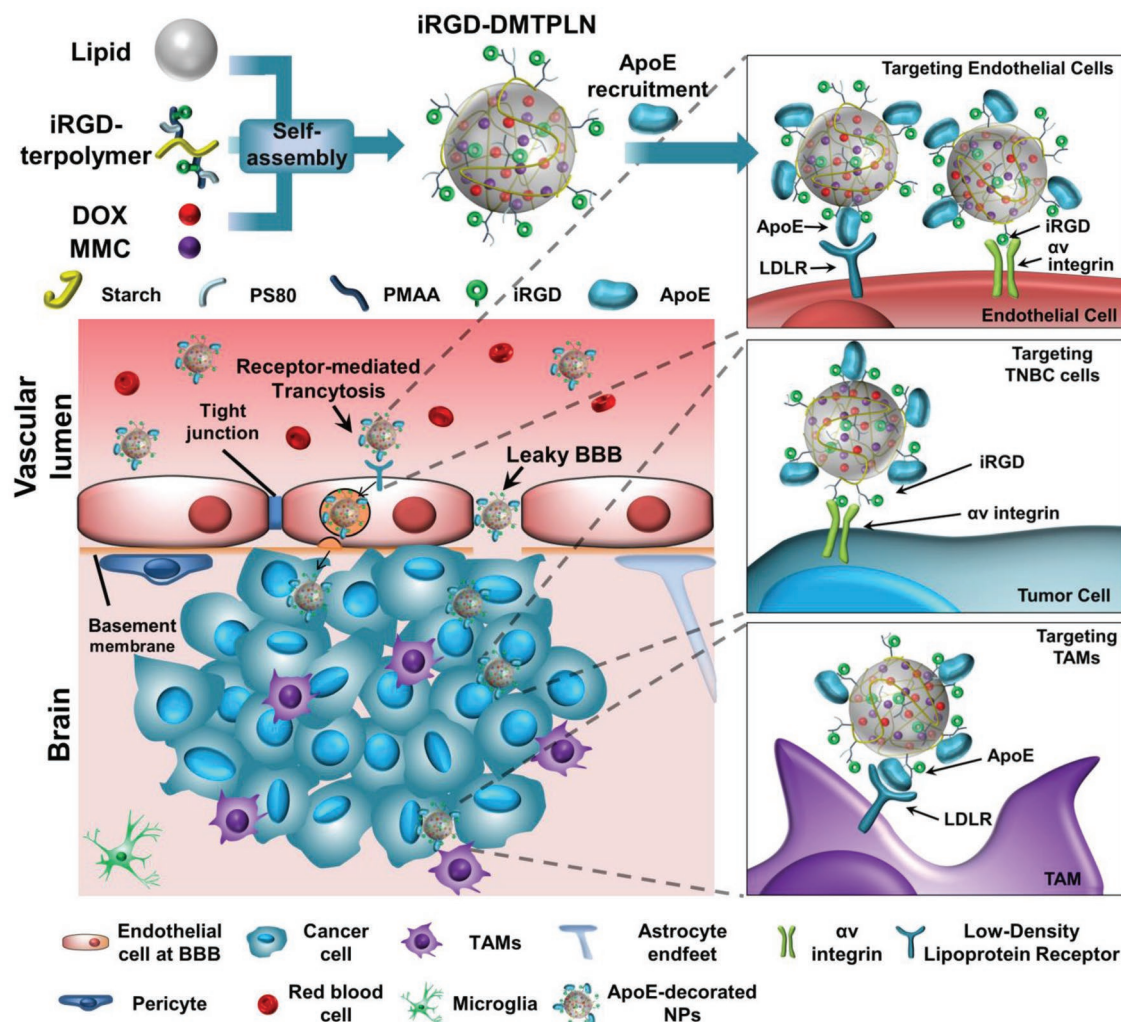
To examine the designed mechanism and multifunctionality of the iRGD-DMTPLN system, we compared cellular uptake, cytotoxicity and targetability of iRGD-free DMTPLN in human TNBC cells and murine RAW 264.7 macrophages in vitro in the absence or presence of an LDLR antagonist. The capability of the iRGD-TPLN crossing the intact BBB was verified by confocal microscopy of brain tissue of healthy mice following intravenous injection of iRGD-DMTPLN loaded with a brain-impermeable nucleus-staining dye. In vivo biodistribution and effects of iRGD-DMTPLN on the TAM population, therapeutic efficacy, and normal tissue toxicity were evaluated using a murine brain metastasis model of human TNBC cells.

2. Results and Discussion

2.1. Synthesis and Characterization of Nanoparticles

The conjugation of iRGD to the terpolymer was made via N-(3-dimethylaminopropyl)-N'-ethylcarbodiimide hydrochloride (EDC)/N-hydroxysuccinimide (NHS) covalent coupling (**Figure 2**a) and confirmed using H^1-NMR (Figure 2b). As highlighted by the blue-dotted box, the new peaks observed in the NMR spectrum of iRGD-terpolymer compared to terpolymer can likely be attributed to protons on the beta- and gamma-carbons of the two cysteines, two arginines and two aspartic acids of the peptide. These proton peaks were slightly shifted to the right side of the spectrum likely due to dipole-dipole interactions between the protons on the peptide and the terpolymer.

Transmission electron micrographs (TEM) images (Figure 2c) portrayed a well-defined spherical nanostructure and confirmed the average particle size measured by the dynamic light scattering method (Figure 2d). The iRGD-DMTPLN have an average particle size of 126 nm, zeta potentials of -43.6 mV, polydispersity index of 0.20, DOX loading efficiencies of 97% and MMC loading efficiencies of 52% (Figure 2e). The properties of DMTPLN are similar to iRGD-DMTPLN (Figure 2e), making the DMTPLN a good control for studying the role of

ADVANCED
SCIENCE NEWS
www.advancedsciencenews.com

ADVANCED
HEALTHCARE
MATERIALS
www.advhealthmat.de

Figure 1. Schematic diagram of self-assembly of iRGD-conjugated terpolymer-lipid nanoparticles with co-loaded DOX and MMC (iRGD-DMTPLN) and proposed mechanism of iRGD-DMTPLN crossing the BBB via synchronized action of ApoE-decorated NP binding to LDLR overexpressed on the endothelial cells at the brain microvessels and iRGD-integrin binding at tumor neovasculature, followed by active targeting to LDLR-expressing TAMs and αv integrins-expressing TNBC cells in the brain metastases.

iRGD conjugation on cellular uptake and cytotoxicity. The number of iRGD peptides on the NPs was estimated to be about 1172 per particle using a fluorometric method as previously described (Table S1, Supporting Information).[8d,22] The colloidal stability of iRGD-DMTPLN and DMTPLN was determined and no significant changes in particle size or zeta potential was observed over 48 h in 50% fetal bovine serum (FBS)-containing α-MEM at 37 °C, or for 7 d in 5% dextrose at 4 °C (Figure S1, Supporting Information). DMTPLN and iRGD-DMTPLN formulations exhibited similar drug release profiles; both gradually released DOX and MMC with ≈80% cumulative release in 72 h (Figure 2f). As the free drug DOX and MMC permeated through the dialysis membrane very quickly, the slow release profiles of the nanoparticle formulations are deemed a consequence of stable polymer-lipid matrix of the nanoparticles.[23] The particle properties and drug release profiles are alike between the two formulations, indicating that the iRGD conjugation did not significantly alter these properties of the

TPLN. Significantly higher fluorescence intensity was observed in iRGD-TPLN-treated $\alpha v\beta 3$ integrin-coated wells compared to TPLN, both loaded with Bodipy (Figure 2g), indicating reserved high affinity of iRGD to $\alpha v\beta 3$ integrin receptor after conjugation with the nanoparticles.

2.2. iRGD-Conjugation Increases the In Vitro Cytotoxicity and Cellular Uptake of DMTPLN in TNBC Cells but Not in Macrophages

The cytotoxicity of iRGD-DMTPLN or DMTPLN against human TNBC MDA-MB-231-luc-D3H2LN and MDA-MB-468 cells and RAW 264.7 murine macrophages was evaluated by 3-(4,5-dimethylthiazol-2-yl)-2,5-diphenyltetrazolium bromide (MTT) assay as a function of DOX/MMC concentration at a fixed DOX:MMC molar ratio of 1.0:0.7 (**Figure 3**a,b, Figure S2a, Supporting Information). Both NP formulations
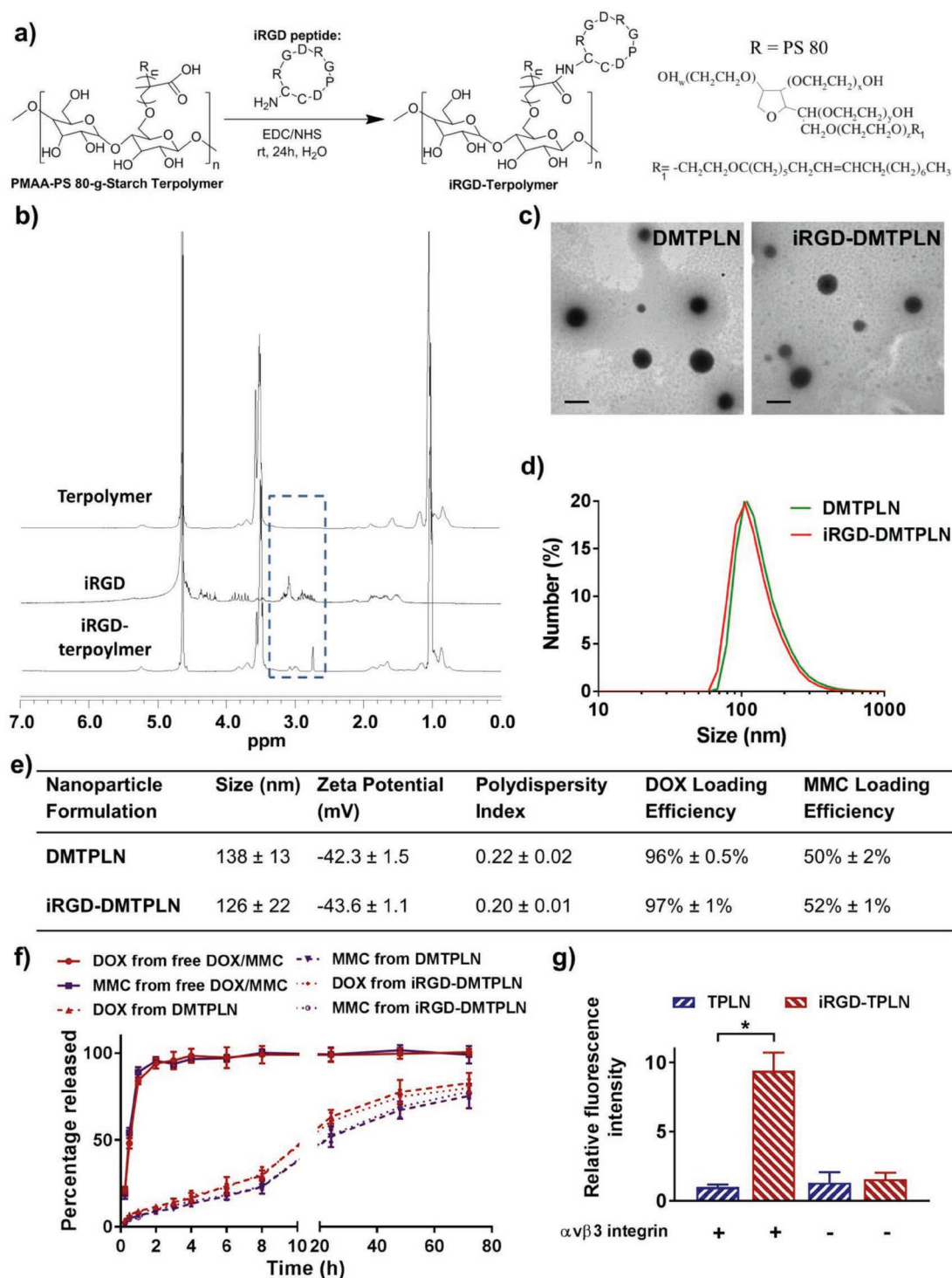
Figure 2. a) Reaction schematic for the conjugation of iRGD and terpolymer, and structure of polysorbate 80 (PS 80). b) H^1-NMR of iRGD peptide, terpolymer, and iRGD-terpolymer. Blue dashed rectangle indicates the perservation of CH$_2$ peaks from the peptide at ≈3.0 ppm. c) Particle size distribution. d) TEM images. Scale bar = 200 nm. e) Summary table of NP properties. f) Release profiles of DOX and MMC from DMTPLN and iRGD-DMTPLN in PBS (pH = 7.4) determined by dialysis at 37 °C over 72 h. Data are presented as the mean ± SD ($n = 3$). g) In vitro binding of Bodipy-labeled nanoparticles on immobilized recombinant human $\alpha v \beta 3$ integrin receptors. Data are presented as mean ± SD, $n = 3$. *$p < 0.05$.

increased the cytotoxicity and drug uptake significantly in both cell lines. However, iRGD conjugation only enhanced efficacy of DMTPLN and DOX uptake in the TNBC cells but not in the macrophages that exhibit low integrin expression. The half maximal inhibitory concentration (IC50) of iRGD-DMTPLN in MDA-MB-231 cells (0.42 ± 0.08 µg mL^{-1}) is significantly
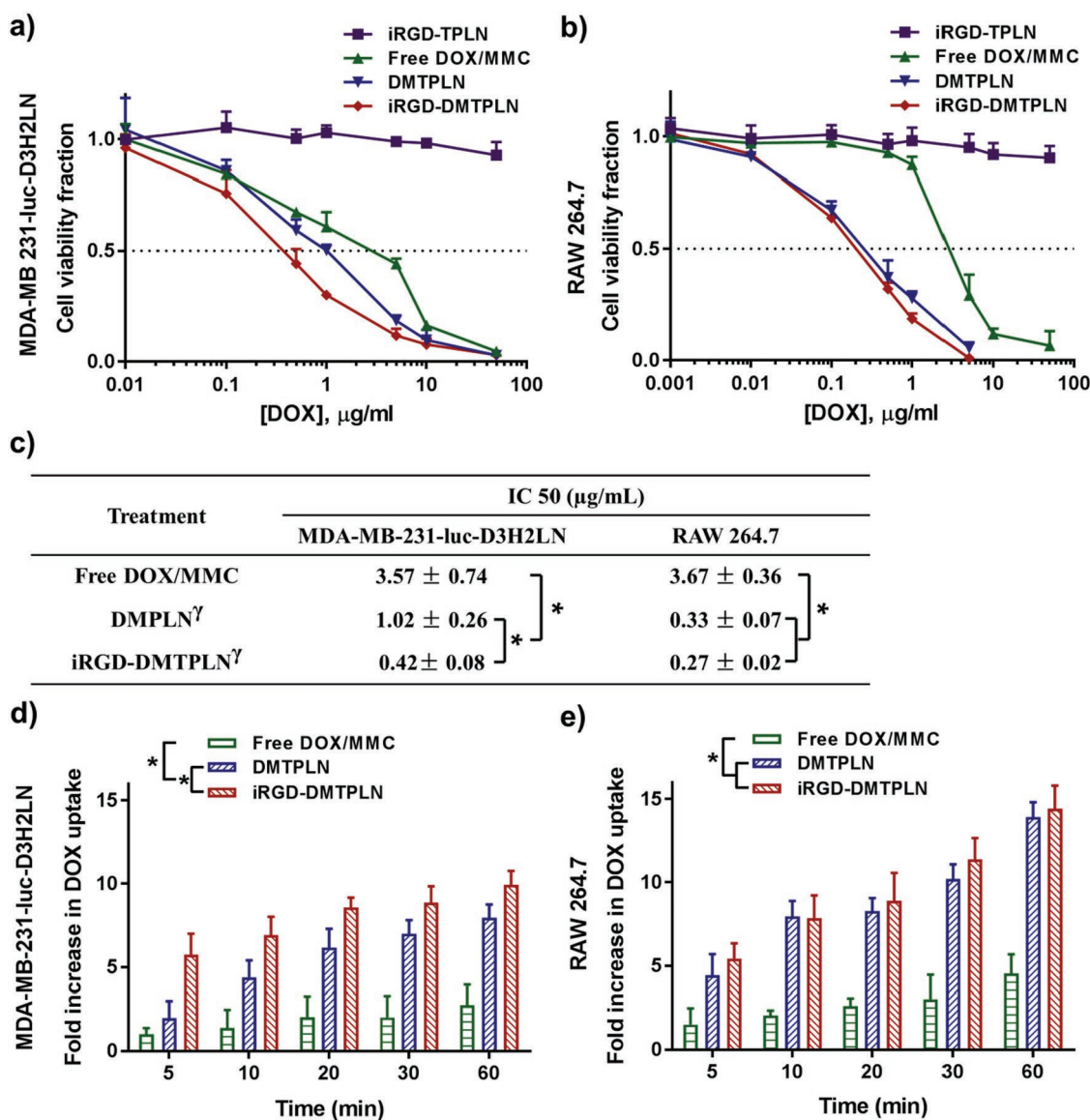
Figure 3. In vitro cytotoxicity and DOX uptake of different formulations of DOX and MMC in human breast cancer cells and murine macrophages. Cytotoxicity of different DOX/MMC formulations in DOX:MMC molar ratio of 1.0:0.7 against a) MDA-MB-231-luc-D3H2LN cells and b) RAW 264.7 macrophages. Cells were treated for 1 h with various DOX/MMC concentrations of free DOX/MMC or DMTPLN or iRGD-DMTPLN, or blank iRGD-TPLN with same concentration of the NP. X-axes based on DOX concentration. Cells were allowed to proliferate for 24 h before being evaluated for viability by MTT assay. c) IC50 of each treatment. d,e) Cellular uptake of DOX in the two cell lines. The fold increase in fluorescence of internalized DOX in cells exposed to free DOX/MMC, DMTPLN, and iRGD-DMTPLN for up to 1 h was evaluated by spectrofluorometry. Fold-change was measured as DOX uptake relative to free DOX uptake in MDA-MB-231-luc-D3H2LN at 5 min. Data are presented as mean ± SD, $n = 3$. $*p < 0.05$. γ indicate significance of $p < 0.05$ between two cell lines.

lower than the IC50 of DMTPLN (1.02 ± 0.26 µg mL^{-1}) and free DOX/MMC (3.57 ± 0.74 µg mL^{-1}) ($p < 0.05$) (Figure 3c). A similar trend was also observed in MDA-MB-468 cells, another TNBC cell line (Figure S2a, Supporting Information). In contrast, iRGD-DMTPLN did not produce higher cytotoxicity in RAW 264.7 macrophages (IC50 0.27 ± 0.02 µg mL^{-1}) compared to DMTPLN (IC50 0.33 ± 0.07 µg mL^{-1}), while both IC50s were significantly lower than that of free DOX/MMC (3.67 ± 0.36 µg mL^{-1}) ($p < 0.05$) (Figure 3c). The in vitro cytotoxicity results (Figure 3a–c, Figure S2, Supporting Information) demonstrate that DMTPLN and iRGD-DMTPLN

are significantly more cytotoxic to RAW 264.7 macrophages (IC50 0.33 ± 0.07 and 0.27 ± 0.02 µg mL^{-1}, respectively) than to the human TNBC cells with IC50 1.02 ± 0.26 and 0.42 ± 0.08 µg mL^{-1}, respectively in MDA-MB-231-luc-D3H2LN cells ($p < 0.05$) (Figure 3c).

To elucidate a possible explanation for the differences in IC50s between formulations and cell lines, levels of DOX in the cells treated with various formulations over a period of 1 h were examined by measuring its fluorescence intensity. In line with the trend of cytotoxicity presented above, nanoparticle formulations, i.e., DMTPLN and iRGD-DMTPLN significantly increased

ADVANCED
SCIENCE NEWS
www.advancedsciencenews.com

ADVANCED
HEALTHCARE
MATERIALS
www.advhealthmat.de

DOX uptake in both cell lines. However, iRGD-conjugation resulted in a higher DOX level in MDA-MB-231-luc-D3H2LN cells treated with iRGD-DMTPLN compared to DMTPLN ($p < 0.05$) (Figure 3d); whereas iRGD conjugation did not affect DOX uptake by RAW 264.7 macrophages (Figure 3e). It is worth noting that DOX levels in RAW 264.7 macrophages delivered by both nanoparticle formulations were significantly higher (≈14-fold increase from free DOX at 60 min) than that in MDA-MB-231-luc-D3H2LN cells (8–10-fold increase at 60 min), possibly due to their strong phagocytic activity mediated by surface receptors such as LDLR.[24]

The iRGD conjugation facilitated DOX uptake was also observed in MDA-MB-468 cells (Figure S2b,c, Supporting Information) and confirmed microscopically in both human TNBC cell lines (Figure S2d, Supporting Information). The positive effect of iRGD conjugation on DOX uptake and cytotoxicity in the human TNBC cells is possibly due to integrin-mediated endocytosis of iRGD-DMTPLN via αv integrins overexpressed on both cell lines.[19b,c] In RAW 264.7 macrophages, indistinguishable drug uptake and cytotoxicity between DMTPLN and iRGD-DMTPLN are ascribed to the lack of αv integrin overexpression.[25]

2.3. Effect of LDLR Inhibition on Nanoparticle Uptake In vitro

It is known that LDLRs are highly expressed on MDA-MB-231-luc-D3H2LN cells and RAW 264.7 macrophages.[19d,26] However it is unknown whether their overexpression leads to additional targeting specificity of nanoparticles or whether the designed iRGD-TPLN could target both integrins and LDLR. It is anticipated that PS 80-containing TPLN could target the LDLR via recruiting apolipoproteins onto the NP surface.[17b,c] We first investigated this mechanism in vitro by pretreating the cells with an LDLR antagonist, receptor-associated proteins (RAPs), prior to incubation with DMTPLN or iRGD-DMTPLN. RAP pretreatment diminished cellular uptake of fluorescent dye-labeled DMTPLN in both cell lines measured by spectrofluorometry (**Figure 4**a) and by confocal microscopy (Figure 4b); but its antagonizing effect on cellular uptake of iRGD-DMTPLN was less significant in MDA-MB-231-luc-D3H2LN cells than in RAW 264.7 macrophages. These results indicate that LDLR-mediated endocytosis plays a more important role in nanoparticle uptake of iRGD-DMTPLN in the macrophages than the TNBC cells; and integrin-iRGD interaction remains a main mechanism for NP uptake of
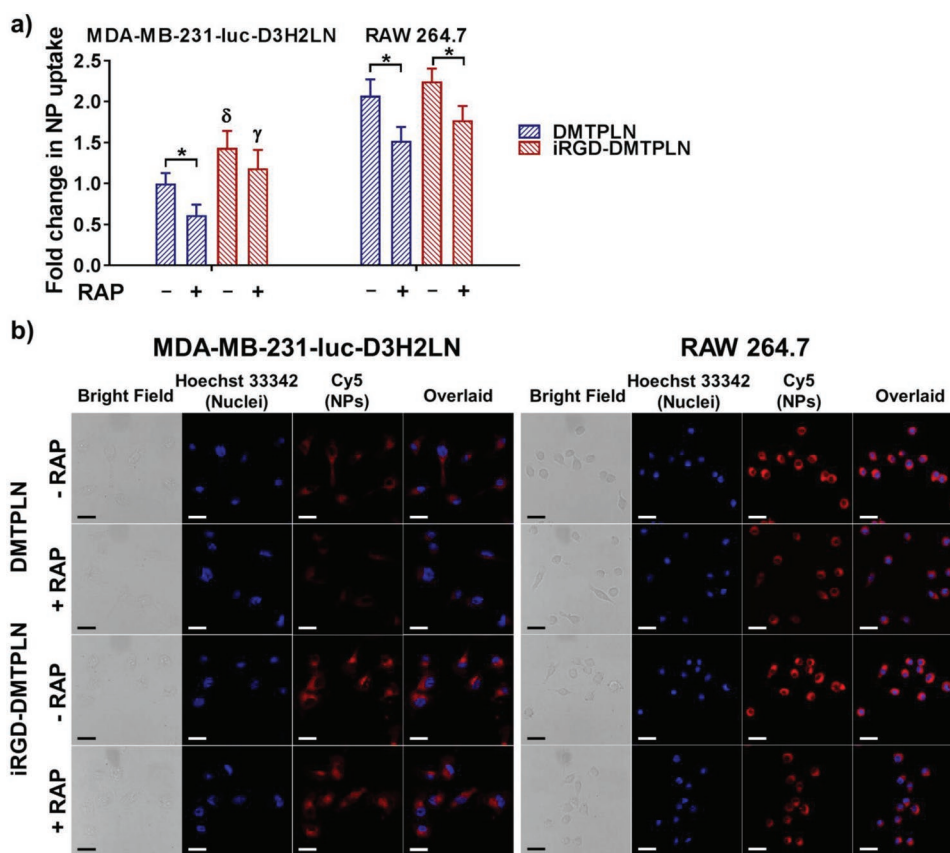
Figure 4. Effect of LDLR inhibition on the uptake of NPs in MDA-MB-231-luc-D3H2LN cells and RAW 264.7 macrophages. Cells were incubated with fluorescent Cy5-labeled DMTPLN or iRGD-DMTPLN for 1 h with or without pretreatment of the LDLR inhibitor RAP for 1 h. a) The fold increase in fluorescence of internalized NPs was measured by spectrofluorometry. All fold changes in fluorescence were relative to fluorescence of MDA-MB-231-luc-D3H2LN cells treated with DMTPLN without pretreatment of RAP. Data are presented as mean ± SD, $n = 3$. *$p < 0.05$. δ and γ indicate significant difference between iRGD-DMTPLN and DMTPLN treated group with or without RAP treatment. b) Confocal microscopic images of internalized fluorescent NPs. Scale bars = 30 µm

iRGD-DMTPLN in MDA-MB-231-luc-D3H2LN cells. Partial inhibition of DMTPLN and iRGD-DMTPLN uptake by RAP suggests that other internalization pathways may exist in addition to LDLR-mediated endocytosis, or that RAP does not completely block LDLR-mediated uptake. Higher NP uptake by RAW 264.7 macrophages compared to MDA-MB-231-luc-D3H2LN cells is consistent with the DOX uptake shown in Figure 3d,e.

2.4. iRGD-DMTPLN Deliver BBB-Impermeable Agents into Healthy Brain

The ability of the PS 80-containing iRGD-conjugated NPs to cross the BBB and deliver brain-impermeable agents into healthy brain was assessed by intravenous injection of various formulations containing a brain-impermeable dye (Hoechst 33342) that stains cell nuclei. Confocal laser scanning microscopic images showed that iRGD-DMTPLN and DMTPLN with covalently bound PS 80 crossed the BBB and delivered the dye and DOX to brain parenchyma; whereas treatments with PS 80-free iRGD-DMPLN, or free dye plus DOX, showed no DOX accumulation outside of brain blood vessels, and stained only blood vessel-associated cell nuclei (**Figure 5**). This result is consistent with our previous findings with the terpolymer-based NP systems and suggests that PS 80, but not iRGD, contributes to the brain-penetrating ability of iRGD-DMTPLN to cross the intact BBB.[17b,c] Several studies

have reported that iRGD-conjugated NP delivery systems are able to deliver drugs or imaging agents to the brain; however, those studies were conducted in murine brain tumor or metastasis models with impaired BBB that enables the enhanced permeation and retention (EPR) effect.[27] The present study suggests that iRGD is unlikely to facilitate receptor-mediated BBB-crossing in healthy brain.

2.5. iRGD Conjugation Increases Nanoparticle Accumulation in Brain Metastasis

The biodistribution and brain accumulation of iRGD-DMTPLN were further investigated in a murine MDA-MB-231-luc-D3H2LN brain metastasis model. Two weeks after intracranial inoculation of the cancer cells, the mice were intravenously injected with a near-infrared dye, HiLyte Fluor 750 (HF 750)-labeled NPs with or without iRGD conjugation. Whole body biodistribution of NPs was monitored for up to 2 h postinjection using a Xenogen imager (Dorsal view: **Figure 6**a; Ventral view: Figure S4, Supporting Information). Stronger fluorescence signal of HF750-NPs was observed in the brain of metastasis-bearing mice treated with iRGD-DMTPLN than in the DMTPLN-treated mice. Ex vivo brain imaging revealed co-localization of DOX signal, HF 750 signal and tumor bioluminescence signal in the mice treated with the two NP formulations, while minimal DOX signal was observed in the mice treated with free drugs (Figure 6b).
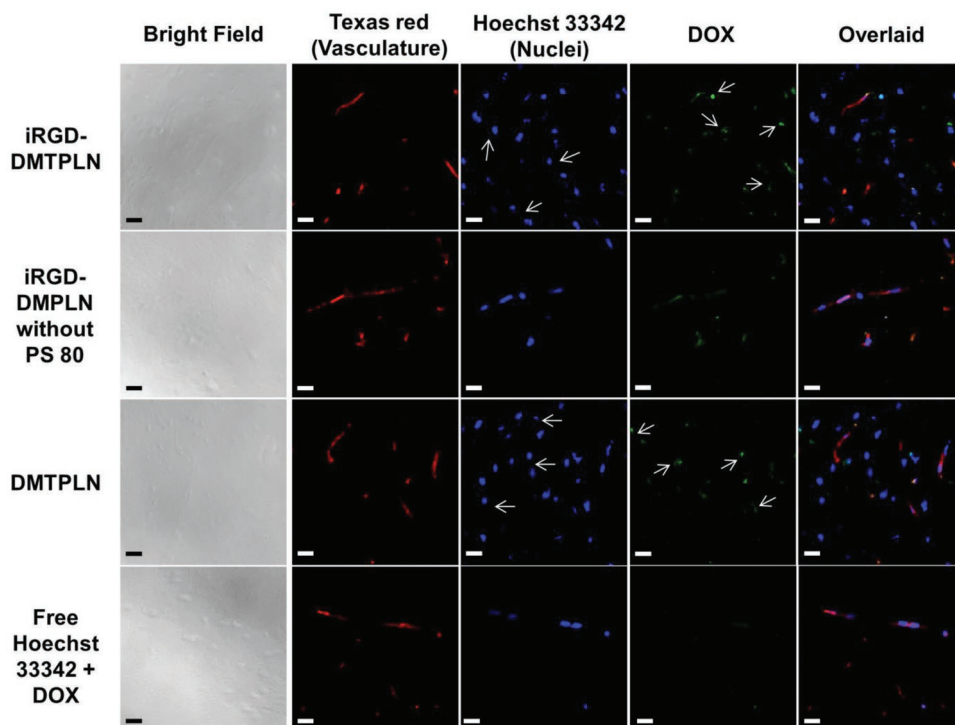
Figure 5. Laser scanning confocal microscopic images of brain sections from healthy NRG mice treated with Hoechst 33342-loaded iRGD-DMTPLN, iRGD-DMPLN (without PS 80), DMTPLN, or free Hoechst 33342 + free DOX/MMC for 2 h. Overlaid images contain the stained vasculature, nuclei, and DOX. Blood vessels were labeled red by intravenous administration of Texas Red-dextran 15 min before euthanasia. Hoechst 33342-labeled cell nuclei appear blue. DOX appears green. Arrows indicate representative stained nuclei and DOX located away from blood vessels. Scale bars = 20 µm.
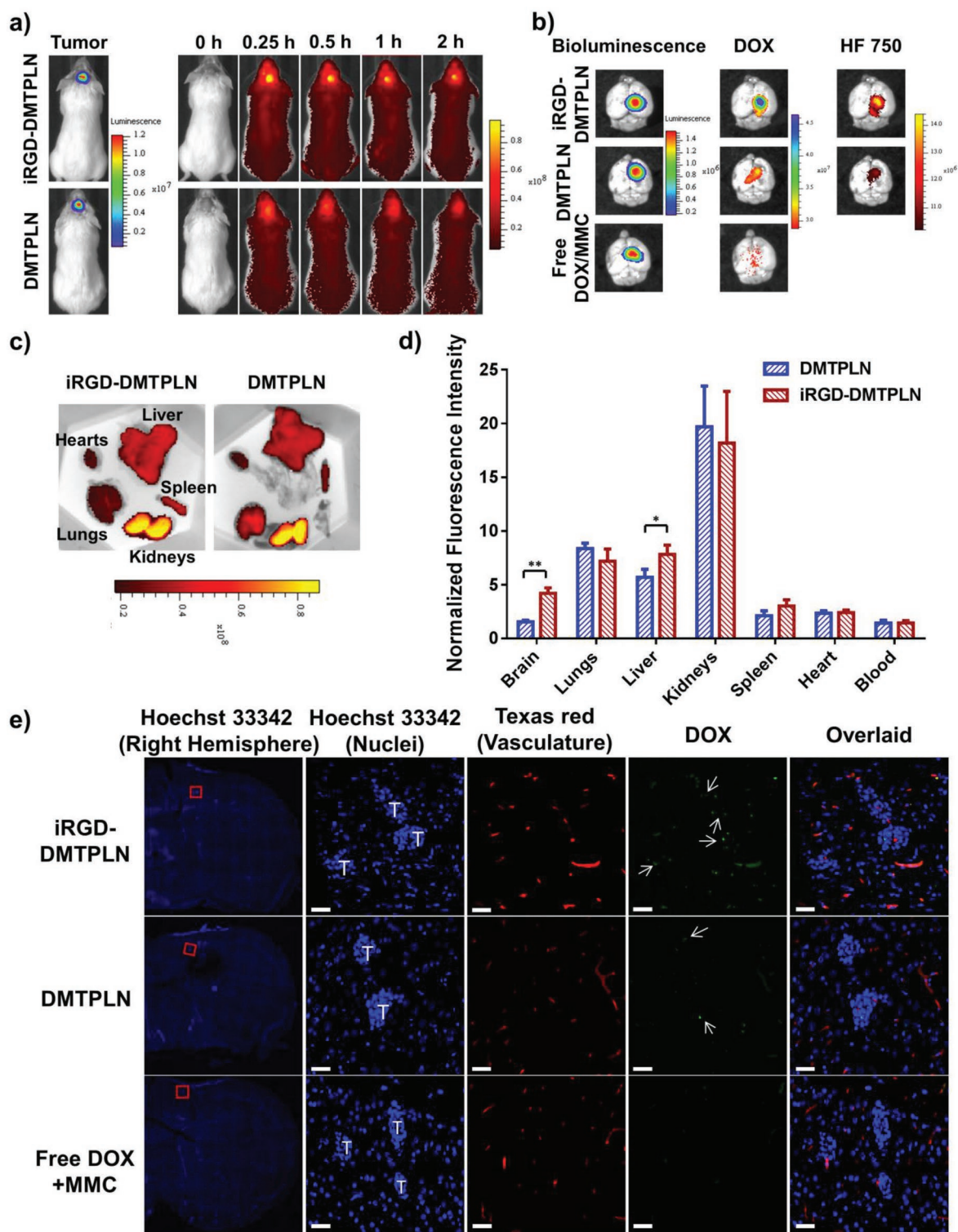
Figure 6. Biodistribution of HF 750-labeled DMTPLN and iRGD-DMTPLN in the NRG mice model of MDA-MB 231-luc-D3H2LN TNBC brain metastasis. a) Whole body biodistribution images up to 2 h using Xenogen IVIS Spectrum System 100 with excitation at 745 nm and emission at 820 nm. b) Ex vivo image of fluorescence signals of NPs and DOX and tumor bioluminescence in the brain. c) Representative qualitative presentation of organ biodistribution ex vivo at 2 h. d) Quantitative presentation of ex vivo organ biodistribution at 2 h. Data are presented as mean ± SD, $n = 3$. *$p < 0.05$ and **$p < 0.005$. e) Laser scanning confocal microscopic images of brain sections from metastasis-bearing NRG mice treated for 2 h. Area with brain metastases indicated by red box was enlarged. Letter "T" indicates metastatic tumors. Scale bars = 40 μm. Overlaid images contain the stained vasculature, nuclei and DOX. Blood vessels were labeled red by intravenous administration of Texas Red-dextran 15 min before euthanasia. Hoechst 33342-labeled nuclei appear blue. DOX appears green. Arrows indicate representative DOX located away from blood vessels.

**ADVANCED
SCIENCE NEWS**
www.advancedsciencenews.com

**ADVANCED
HEALTHCARE
MATERIALS**
www.advhealthmat.de

Based on fluorescence intensity, iRGD-DMTPLN were capable of delivering a higher amount of DOX and HF 750 to the brain metastasis compared to DMTPLN (Figure 6b,d), suggesting that iRGD enables more effective NP targeting to the brain metastases. The increased fluorescence signal in the kidneys might be ascribed to the renal clearance of released HF 750-labeled polymer chains (Figure 6c,d). Slightly higher liver uptake of iRGD-DMTPLN than DMTPLN is likely due to the recognition of RGD peptide on the NPs by the reticuloendothelial system.[7b,8d]

DOX delivery by iRGD-DMTPLN or DMTPLN to brain metastases was further evaluated microscopically. The fluorescent and H&E stained imaged of brain revealed numerous spontaneous small-sized metastatic lesions throughout the brain, including the cortex and subcortex in the brain metastasis model (Figure 6e, Figure S3, Supporting Information). Confocal fluorescence images of brain samples obtained at 2 h post-treatment revealed more dots of DOX and much brighter DOX fluorescence signal in the iRGD-DMTPLN treatment group than the DMTPLN group; while free DOX-MMC treated group did not show DOX signal in the brain (Figure 6e). The microscopic results further confirm the enhanced drug delivery to brain metastases by iRGD-conjugation to DMTPLN depicted in whole body and ex vivo images (Figure 6a–d). In addition, higher fluorescent intensity of Texas red staining vasculature was observed in the iRGD-DMTPLN group compared to DMTPLN, attributable to higher binding of iRGD-DMTPLN to the integrin-overexpressing tumor neovasculature, which may increase the retention of the injected Texas red-dextran by the interaction of iRGD-DMTPLN with Texas red-dextran.

Various iRGD conjugated NPs and iRGD-drug conjugates have been reported to bind αv integrin-overexpressing cells with high affinity.[28] The present combined results delineated the mechanism by which iRGD-DMTPLN sequentially overcome each barrier to deliver drugs to brain metastasis. First, iRGD-DMTPLN extravasates from blood vessels via the aforementioned BBB-penetrating mechanism involving PS 80, ApoE, and LDLR. Additionally, iRGD-DMTPLN may also bind to αv integrin overexpressing tumor vasculature, concentrating near the metastatic tumor, and enhancing BBB penetration via an iRGD-mediated trancytosis mechanism involving iRGD binding to αv integrin and neuropilin-1.[9] Second, once iRGD-DMTPLN leaves the vasculature, they can actively target αv integrin-overexpressing MDA-MB-231-luc-D3H2LN tumor cells. While iRGD-DMTPLN may not be completely intact after crossing the BBB, active targeting is still present because iRGD is covalently conjugated to the terpolymer chain.

### 2.6. iRGD-DMTPLN Reduce TAM Population in TNBC Metastases-Bearing Brain

Given the ability of iRGD-DMTPLN to cross the BBB tumor vasculature and target LDLR-overexpressing macrophages in vitro, its effect on TAMs in the metastatic microenvironment was investigated. Three weeks after intracranial inoculation of brain metastases with MDA-MB-231-luc-D3H2LN cells, the mice were intravenously treated with saline, free

drugs, DMTPLN or iRGD-DMTPLN. At day 3 post-treatment, mouse brains were resected, sectioned and immunohistochemically stained for TAMs (using anti-F4/80 antibody) and microglia (using anti-TMEM119 antibody). The images showed that DMTPLN and iRGD-DMTPLN-treated mice greatly reduced F4/80 positive TAMs compared to the saline- and free drug-treated groups (**Figure 7**a). Quantification of F4/80-positive areas in the metastasis regions illustrated that DMTPLN (4.2 ± 2.3%) and iRGD-DMTPLN (1.4 ± 1.0%) formulations significantly decreased TAMs compared to saline control (16.3 ± 2.3%) and free DOX/MMC (9.9 ± 1.9%) groups (Figure 7b). Despite the existence of subpopulation of tumoricidal TAMs, the overall function of TAMs is protumoral, where they stimulate angiogenesis, promote metastasis and suppress immune response.[29] Therefore, the depletion of TAMs by DMTPLN or iRGD-DMTPLN might translate into enhanced anticancer efficacy. The inhibitory effect of the NPs on TAM density is likely due to the targeted drug delivery of PS 80-containing DMTPLN and iRGD-DMTPLN to the LDLR-overexpressing TAMs as demonstrated in vitro (Figure 4).[19f] The treatment with iRGD-DMTPLN resulted in a more reduction in F4/80 positive area compared to DMTPLN treatment, though the difference was not statistically significant (Figure 7b). Although macrophages do not overexpress αvβ3 integrin, their baseline expression of αvβ3 was reported to enable RGD peptide targeting to reduce TAM recruitment in a murine glioblastoma xenografts model.[25,30] Thus, in addition to delivering more drugs to the metastatic microenvironment, iRGD-DMTPLN may also inhibit TAM recruitment, resulting in greater TAM reduction as shown in Figure 7.

TAM population within brain tumor microenvironment has been reported to include both tissue-resident microglia and bone marrow-derived macrophages.[11b] In the present study, the low levels of TMEM119+ microglia in the metastasis regions (Figure 7a) indicate that most TAMs were likely recruited from the circulation instead of recruitment from the local microenvironment. The TMEM119 staining showed sparsely distributed star-shaped microglia in metastasis-free brain regions of treated mice, suggesting that the treatment did not reduce the microglial population in noncancerous brain regions. This is likely due to the low toxicity of DNA-damaging drugs (i.e., DOX and MMC) to less proliferative cells, such as microglia, and selective accumulation of the NPs at the site of brain metastases.[31]

2.7. iRGD-DMTPLN Inhibit the Progression of Brain Metastasis and Extend Host Survival

To evaluate the in vivo therapeutic potential of iRGD-DMTPLN, its efficacy was compared to the blank nanoparticles iRGD-TPLN, free DOX/MMC and DMTPLN based on a two-intravenous dose regimen (**Figure 8**a). Based on the dose tolerance study, the free DOX/MMC at 6 mg kg^{-1} DOX dose was tolerable with no significant body weight loss (Figure 8d), and thus was chosen for efficacy evaluation. Bioluminescence images (Figure 8b,c) and body weights (Figure 8d) were recorded every week for five weeks, and the survival of the treated mice was monitored based on humane end points (Figure 8e). The
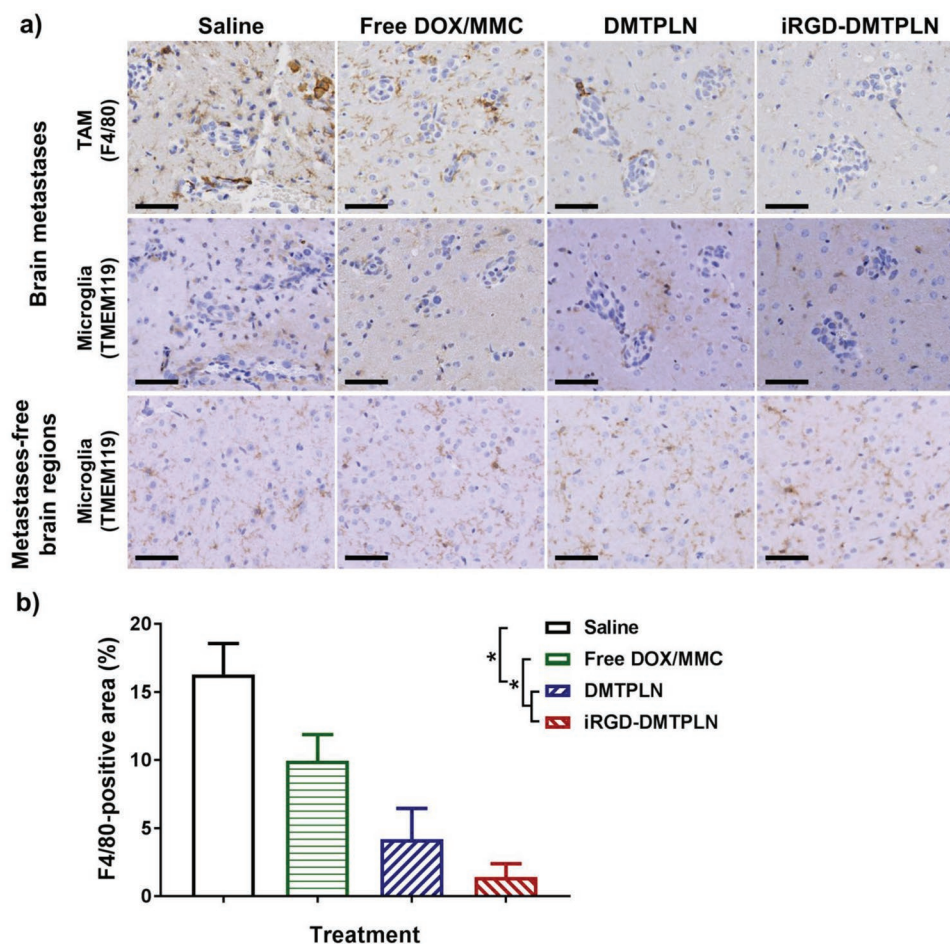
Figure 7. Targeting TAMs with iRGD-DMTPLN in vivo. 3 d following intravenous injection of saline, free drugs, DMTPLN, and iRGD-DMTPLN (6 mg kg^{-1} DOX dose at a DOX/MMC molar ratio of 1:0.7), the metastases-bearing mouse brains were resected for immunohistochemical (IHC) staining of TAMs using anti-F4/80 antibody and microglia using anti-TMEM119 antibody. a) Representative images of the IHC staining are shown. Scale bars = 50 μm. b) Quantification of F4/80-positive areas in metastatic brain regions. Data are presented as mean ± SD, $n = 3$. *$p < 0.05$.

fold-change in tumor bioluminescence radiance (FC-TBR) was compared to that at day 0 as a measure of metastatic burden. iRGD-DMTPLN treatment significantly reduced FC-TBR at day 28 by ≈6-fold and ≈19-fold compared to DMTPLN ($p < 0.05$) and free drugs ($p < 0.05$) (≈4-fold compared to saline) treatment, respectively (Figure 8c). No significant acute weight losses from the treatments were observed, and the weight losses at later stage were likely due to the progression of brain metastases (Figure 8d). iRGD-DMTPLN treatment significantly extended the median survival time of brain metastasis-bearing mice by 58% and 28% compared to free drugs ($p < 0.005$) and DMTPLN ($p < 0.05$) treatment, respectively (Figure 8e,f). Improved therapeutic efficacy of iRGD-DMTPLN is attributed to greater amounts of drugs delivered to the metastases via the sequential triple targeting of the BBB, cancer cells and TAMs.

2.8. iRGD-DMTPLN Exhibit No Significant Acute Toxicity to Major Organs

Cardiotoxicity is a well-known limitation to the therapeutic use of DOX.[32] To determine whether the current NP formulations

of DOX/MMC can reduce the toxicity of the drug combination compared to free drugs, heart, liver, kidneys and lungs were collected from brain metastasis-bearing mice for histopathological examination 3 d after treatment with saline, free DOX/MMC, DMTPLN or iRGD-DMTPLN at a DOX dose of 6 mg kg^{-1}. H&E staining showed that DMTPLN and iRGD-DMTPLN did not cause any observable toxicity compared to saline control. Free DOX/MMC treatment resulted in myocardial vacuolation in the ventricle wall, but no observable toxicity to the liver, kidneys and lungs (Figure S5a, Supporting Information).[33] Increased serum level of cardiac troponin I was observed in the free DOX/MMC group compared to the other three groups, though the difference was not significant (Figure S5b, Supporting Information). The reduced cardiotoxicity of the DOX/MMC combination by iRGD-DMTPLN and DMTPLN is attributable to the selected drug delivery to tumor sites and local drug release.

3. Conclusion

A novel triple targeted, iRGD-modified terpolymer-lipid nanoparticle (iRGD-TPLN) system was designed to deliver
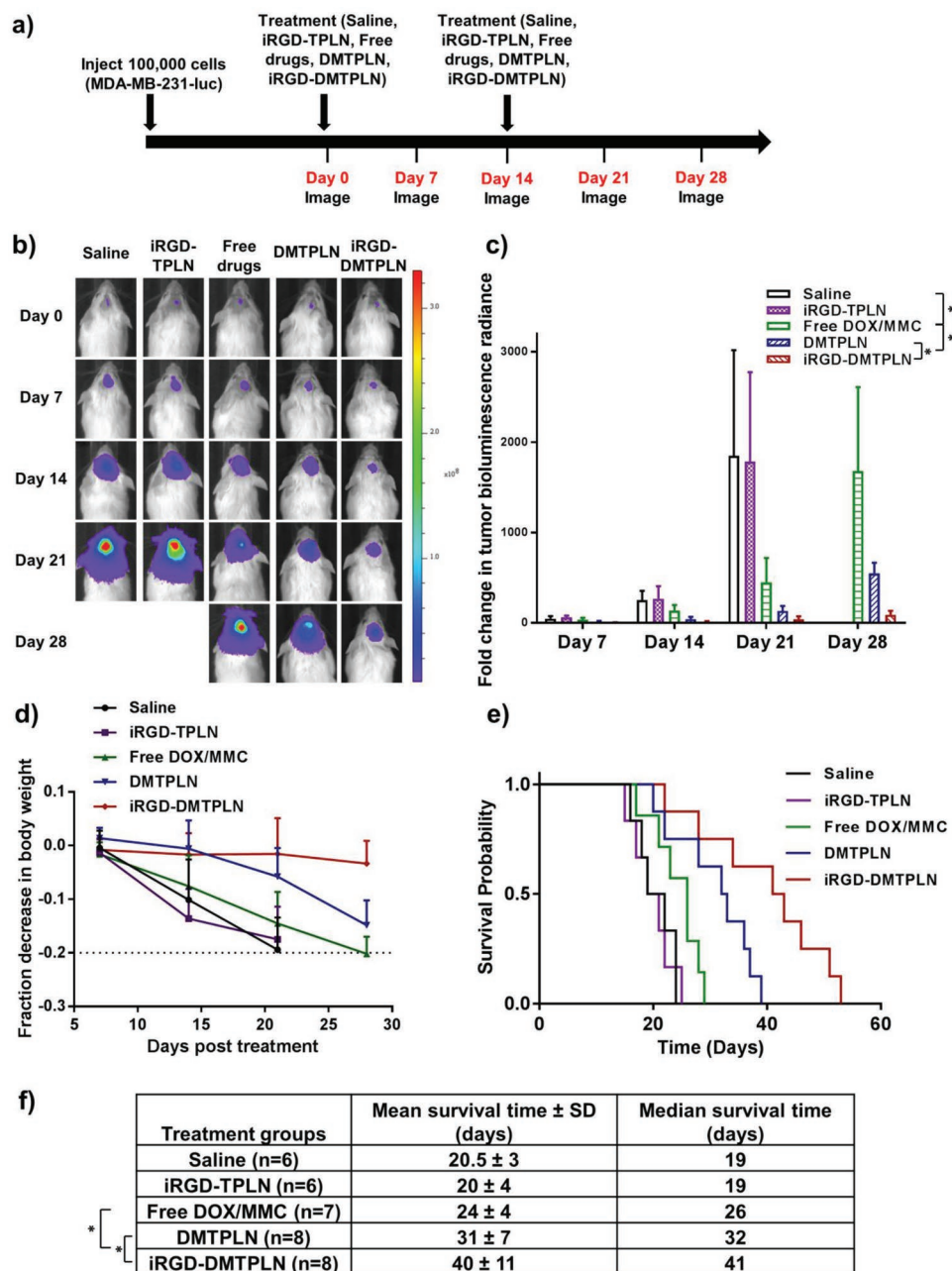
Figure 8. MDA-MB-231-luc-D3H2LN brain metastases-bearing NRG mouse tumor growth and survival. a) Treatment and imaging schedule for tumor-bearing mice injected with saline ($n = 6$), blank iRGD-TPLN ($n = 6$), Free DOX/MMC (6 mg kg^{-1} DOX, $n = 7$), DMTPLN (6 mg kg^{-1} DOX, $n = 8$), or iRGD-DMTPLN (6 mg kg^{-1} DOX, $n = 8$). All treatments included MMC in a DOX:MMC molar ratio of 1.0:0.7. b) In vivo bioluminescence images of representative brain metastases images over 28 d. c) Tumor burden measured by fold change in tumor bioluminescence radiance (FC-TBR) at days 7, 14, 21, and 28. d) Changes in mice body weight of treated group. Mice with body weight loss that were below the dotted line of 20% were euthanized according to the Animal Care Committee guidelines. e) Kaplan–Meier survival plot, and f) mean and median survival time of each treatment group of brain metastases-bearing mice. FC-TBR and body weight loss are presented as mean ± SD. *$p < 0.05$.

synergistic anticancer drugs DOX and MMC across the BBB and target TNBC brain metastases and TAMs. The rationally designed system utilized the LDLR and integrin binding moieties to enhance BBB penetration by interacting with brain endothelial cells and tumor neovasculature and to target TAMs and TNBC cells in the micrometastases. The capability of iRGD-DMTPLN crossing intact BBB was also demonstrated

in healthy mice. The iRGD-DMTPLN system showed selective targetability to human TNBC cells and murine macrophages via iRGD- and LDLR-mediated mechanisms, respectively, by the in vitro cellular uptake and cytotoxicity studies. The iRGD-DMTPLN system enhanced drug delivery to brain metastases and reduced TAM populations therein and exhibited superior efficacy over DMTPLN or free drugs in terms of tumor growth

ADVANCED
SCIENCE NEWS
www.advancedsciencenews.com

ADVANCED
HEALTHCARE
MATERIALS
www.advhealthmat.de

inhibition and survival of brain metastasis-bearing mice. These results demonstrate that iRGD-DMTPLN is a promising drug delivery system for the treatment of brain metastases of TNBC.

4. Experimental Section

Materials: Soluble corn starch, methacrylic acid (MAA), sodium thiosulfate (STS), potassium persulfate (KPS), polysorbate 80 (PS 80), sodium dodecyl sulphate (SDS), fluoresceinamine isomer I (FA), EDC, NHS, dodecylamine, ethyl arachidate, 9,10-phenanthrenequinone, and all other chemicals unless otherwise mentioned were purchased from Sigma-Aldrich Canada (Oakville, ON, Canada). Cyclic peptide iRGD [c(CRGDRGPDC)] was purchased from LifeTein (Somerset, NJ, USA). HiLyte Fluor 750 hydrazide (HF 750) was purchased from AnaSpec (Fremont, CA, USA). Texas red-labeled dextran (MW 70000 Da) was obtained from Life Technologies (Carlsbad, CA, USA). Hoechst 33342 was purchased from Molecular Probes, Inc. (Eugene, OR, USA). MMC and DOX were purchased from MedChemExpress (Monmouth Junction, NJ, USA). Human and mouse RAPs were purchased from R&D systems (Minneapolis, MN, USA). The MDA-MB-231-luc-D3H2LN cell line was purchased from Caliper Life Sciences (Hopkinton, MA, USA) and MDA-MB-468 is a kind gift from Dr. Mark D. Minden at the Princess Margaret Cancer Centre (Toronto, ON, Canada). RAW 264.7 cells (ATCC TIB-71) were purchased from ATCC (Manassas, VA). All cell lines used were confirmed to be pathogen free by the supplier using IMPACT Profile I (PCR). The cancer cells were passaged for <6 months following recovery from frozen stock, and RAW 264.7 cells were used at less than 20 passages.

Synthesis and Characterization of DOX and MMC Coloaded Terpolymer-Lipid Nanoparticles: The starch-based terpolymer was synthesized to contain a pharmaceutical excipient, PS 80, and poly(methacrylic acid) (PMAA) (PMAA-PS 80-g-St) following previously reported methods.[34] TPLN was then prepared using a one-pot self-assembly method.[17b,c] Briefly, to a solution of 12 mg of ethyl arachidate and MMC (100 μL, 8 mg mL^{-1}, in methanol) preheated to 65 °C, Pluronic F-68 (PF 68) (50 μL, 100 mg mL^{-1}), DOX (100 μl, 10 mg mL^{-1}), and PMAA-PS 80-g-St terpolymer (200 μL, 50 mg mL^{-1}) in distilled deionized (DDI) water were added and stirred for 20 min. The suspension was emulsified at 65 °C at 100% peak power for 10 min using a Hielscher UP 100H probe ultrasonicator (Ringwood, NJ, USA). The emulsion was then quickly transferred into 1 mL of saline being stirred on ice to generate DMTPLN. To synthesize iRGD-DMTPLN, iRGD-terpolymer, prepared by covalently linking iRGD peptides to PMAA chains of terpolymer via NHS/EDC (N-hydroxysuccinimide/1-Ethyl-3-(3-dimethylaminopropylcarbodiimide) at an iRGD/terpolymer ratio of ≈30 nmol mg^{-1}, was used instead of unconjugated terpolymer followed by the same process. Particle size and zeta potential were measured with a Malvern Zetasizer Nano ZS (Worcestershire, UK). The DOX and MMC coloaded NP suspensions were centrifuged at 8000 g for 15 min through a 0.1 μm filter unit (Millipore, Etobicoke, ON, Canada) to remove the particle encapsulated drugs. The free drug concentration in the filtrate was assayed spectrophotometrically (Molecular Devices, San Jose, CA, USA) to calculate the drug loading (% wt encapsulated drug/wt NPs) and encapsulation efficiency (% wt encapsulated drug/wt total drug). The release profiles of DOX and MMC from iRGD-DMTPLN in phosphate-buffered saline was determined by a dialysis method using a dialysis membrane (Spectrum Laboratories, Inc. Rancho Dominguez, CA, USA) with a 12 kDa molecular weight cut-off (MWCO). DMTPLN, iRGD-DMTPLN and free DOX/MMC solutions all contained the two drugs, DOX and MMC, at a molar ratio of 1.0:0.7.[8d,20b]

An in vitro binding assay was performed to evaluate the binding of iRGD-conjugated nanoparticles to $\alpha v\beta 3$ receptor as previously described.[7b,35] A 96-well high binding microtiter plate (Corning, Inc., Corning, NY, USA) was coated with 1 μg mL^{-1} Human integrin $\alpha v\beta 3$ receptor protein (R&D systems, Minneapolis, MN, USA) in Supplemented Tris Buffer (STB, 20×10^{-3} M Tris-HCl (pH 7.4) with

150×10^{-3} M NaCl, 1×10^{-3} M MnCl$_2$, 2×10^{-3} M CaCl$_2$, and 1×10^{-3} M MgCl$_2$) or protein-free Tris buffer overnight at 4 °C. The wells were further blocked with bovine serum albumin for 3 h at 37 °C followed by washing. Bodipy 493/503-loaded TPLN or iRGD-TPLN was incubated in wells with or without human integrin $\alpha v\beta 3$ receptor protein for 1 h at 37 °C, followed by three washes with STB. The fluorescence intensity of Bodipy 493/503-loaded nanoparticles was assayed spectrophotometrically at excitation and emission wavelengths of 493 and 530 nm.

Cell Culture: Human MDA-MB 231-luc-D3H2LN and MDA-MB-468 cells were grown in cell culture flasks (Corning, Corning, New York, USA) in growth medium made from alpha-modified minimal essential medium (α-MEM) (Gibco-Life Technologies, Burlington, ON, Canada) supplemented with 10% FBS (Invitrogen Inc. Burlington, ON, Canada) at 37 °C in a humidified incubator with 5% CO$_2$ atmosphere. RAW 264.7 were cultured in growth medium made from Dulbecco's Modified Eagle's Medium (D-MEM) (Gibco-Life Technologies, Burlington, ON, Canada) supplemented with 10% FBS under the same condition as TNBC cells.

In Vitro Viability Test: Cells were plated at a density of 10 000 cells per well in 100 μL of respective growth medium in 96-well plates (R&D systems, Minneapolis, MN, USA) overnight for 18 h. Cells were treated with the following formulations at 37 °C and 5% CO$_2$ for 1 h: iRGD-DMTPLN, DMTPLN or free DOX/MMC at equivalent DOX concentrations of 0.001–50 μg mL^{-3} in growth medium. After being washed three times with phosphate-buffered saline (PBS), the cells were incubated in growth medium for a further 24 h. Cell viability was measured using MTT assay. To each well, 100 μL of 1.2×10^{-3} M MTT in α-MEM was added followed by 4 h of incubation at 37 °C. Then, 50 μL of dimethyl sulphoxide (DMSO) was added to each well and incubated for 20 min at 37 °C. The concentration of formazan was analyzed with SpectraMax M2 microplate reader (San Jose, CA, USA) at 540 nm.

In Vitro Cellular Uptake of DOX: To evaluate the cellular uptake of DOX, cells were seeded at a density of 10 000 cells per well in 100 μL of growth medium in black 96-well plates (Sarstedt, Saint Léonard, QC, Canada) and incubated for 18 h at 37 °C, 5% CO$_2$. Free DOX/MMC, iRGD-DMTPLN, or DMTPLN at 5 μg mL^{-3} DOX concentration was added to each well. At 5, 10, 20, 30, and 60 min after the treatment, the medium was removed and the cells were washed three times with PBS. The fluorescence of DOX was measured by SpectraMax M2 microplate reader (San Jose, CA, USA) at λ_{ex} = 490 nm and λ_{em} = 530 nm.[8a] Fold change in DOX uptake was calculated as DOX fluorescence relative to DOX fluorescence in free DOX-treated MDA-MB-231-luc-D3H2LN cells at 5 min.

The uptake of DOX from free DOX/MMC solution, DMTPLN, or iRGD-DMTPLN was also examined in MDA-MB-231-luc-D3H2LN and MDA-MB-468 cells using confocal microscopy. Cells were seeded at densities of 300 000 cells in 3 mL of growth media on 35 mm glass-bottom culture dish (MatTek Corporation, Ashland, OR, USA) and incubated for 24 h in 3 mL of growth medium at 37 °C, 5% CO^2. Cells were then treated with free DOX/MMC, DMTPLN, and iRGD-DMTPLN for 20 min (time is based on the quantitative study of DOX uptake), followed by medium removal. Hoechst 33342 was added for nuclei staining 10 min prior to medium removal. The cells were fixed with 4% paraformaldehyde and washed three times with PBS and imaged with bright field, 405 nm (blue, Hoechst 33342) and 488 nm (green, DOX) using Zeiss LSM 700 laser scanning microscopy (Carl Zeiss Canada, Toronto, ON, Canada).

LDLR Inhibition on Uptake of NPs In Vitro: Terpolymer was covalently conjugated with Cyanine5 (Cy5) amine (Lumiprobe, Hunt Valley, MD, USA) via EDC/NHS coupling. MDA-MB-231-luc-D3H2LN or RAW 264.7 cells were seeded at a density of 10 000 cells per well in 96-well plates in 100 μL 10% human serum (Sigma-Aldrich, Oakville, ON, Canada) or 10% mouse serum (obtained from NRG mice) containing α-MEM or D-MEM, respectively, in black 96-well plates and incubated for 18 h at 37 °C, 5% CO$_2$. The human or mouse serum respectively contains human or mouse ApoE. Cells were preincubated for 1 h with human RAP for MDA-MB-231-luc-D3H2LN cells or mouse RAP for RAW 264.7 cells, an inhibitor for ligand binding to LDLR family, followed by the treatment

of Cy5-conjugated DMTPLN or iRGD-DMTPLN for 1 h. The cells were then washed 3 times with PBS after medium removal. The uptake of fluorescently labeled NPs was measured by microplate reader at $\lambda_{ex} = 600$ nm and $\lambda_{em} = 670$ nm.[17c]

The uptake of NPs was further examined using confocal microscopy. MDA-MB-231-luc-D3H2LN and RAW 264.7 cells were seeded at a density of 15 000 cells per well in 200 µL of culture media on Lab-Tek 8-well chamber slide (Thermo Scientific, Waltham, MA, USA) and incubated for 18 h at 37 °C, 5% CO_2. Cells were preincubated with human or mouse RAP respectively, for 1 h, followed by the treatment of Cy5-conjugated DMTPLN or iRGD-DMTPLN for 1 h. The cells were then fixed by 4% paraformaldehyde and washed 3 times with PBS after medium removal, and imaged with bright field, 405 nm (blue, Hoescht 33342) and 648 nm (red, Cy5-labeled NPs) using Leica TCS SP8 confocal laser scanning microscopy platform (Leica Microsystems, Concord, ON, Canada).

Animal Models: All animal handling and procedures were conducted under an approved protocol from the Animal Care Committee at the Ontario Cancer Institute (Toronto, ON, Canada). An animal model for brain metastasis of triple negative breast cancer was established by injecting luciferase-expressing human breast cancer cells (MDA-MB-231-luc-D3H2LN) (8×10^4 cells per mouse) intracranially into the cortex of four to six week old female NRG mice (Ontario Cancer Institute, Toronto, ON, Canada) using a stereotaxic system (SAS-5100, ASI Instruments, Warren, MI, USA).[17b,c] Intracranial models are commonly used to evaluate therapeutic effect on brain metastasis of breast cancer.[36] Tumor growth was monitored by luciferin-induced bioluminescence imaging (15 mg kg^{-1} luciferin, intraperitoneal injection 10 min prior to imaging) using a Xenogen IVIS spectrum (Caliper Life Sciences, Hopkinton, MA, USA).

Delivery of BBB-Impermeable Dye into Healthy Brain: Hoechst 33342-loaded TPLN was prepared by heating 250 µL of Hoechst 33342 (a nuclear staining fluorescent dye) solution (10 mg mL^{-1} in growth medium), 10 mg of iRGD conjugated terpolymer, 100 µL of 10 mg mL^{-1} DOX solution in DDI, 0.8 mg of MMC, 50 µL of PF 68 solution in DDI (100 mg mL^{-1}), and 12 mg of ethyl arachidate to 65 °C, and stirring for 20 min. NPs were formed under ultrasonication using the same method mentioned in Section 2.2 and suspended in cold sterile saline to a final dye concentration of 2.5 mg mL^{-1}. Furthermore, two additional control formulations were created using procedures described in Section 2.2—iRGD-DMPLN without PS 80 were prepared from iRGD conjugated PMAA-g-St polymer without PS 80, and DMTPLN were prepared from PMAA-PS 80-g-St terpolymer. To examine NP penetration into the healthy brain, healthy NRG mice were treated with 200 µL of dye-loaded iRGD-DMTPLN, iRGD-DMPLN without PS 80, DMTPLN, or free dye + DOX/MMC solution (2.5 mg mL^{-1} dye and 1 mg mL^{-1} DOX in all formulations) via tail vein injection. Mice were euthanized 2 h following treatment. Texas red-labeled dextran (70 000 MW) (100 µL volume, 1 wt% solution) was administered intravenously 15 min prior to euthanasia. The brain was dissected, fixed in 10% formalin for 3 h, transferred to 30% sucrose solution overnight. Ten µm frozen sections were prepared, and the brain cortex was analyzed using Zeiss LSM700 confocal microscope (Carl Zeiss, Jena, Germany) using appropriate fluorescent excitation filters for detection of the indicated chromophores (Texas red-dextran: 555 nm; DOX: 488 nm; Hoechst 33342: 405 nm).[17b,c]

In Vivo Biodistribution Study: Two weeks after tumor cell inoculation in the brains of NRG mice, 200 µL of HF 750-covalently labeled DMTPLN or iRGD-DMTPLN were injected into the lateral tail vein of mice. Biodistribution of the NPs was recorded at various time points up to 2 h with excitation and emission wavelengths of 745 and 820 nm, respectively, using the Xenogen imager. The liver, spleen, kidneys, heart, lungs and blood were then excised and immediately imaged with the imager at 2 h. The fluorescence intensity emitted was quantified with Living Image software over the region of interest (ROI). The fluorescence signals of HF 750-conjugated NPs from major organs were quantified and presented as fold-change from their respective background signal.

Microscopic Analysis of Nanoparticle Distribution in the Brain Metastases: Free DOX/MMC, DMTPLN, or iRGD-DMTPLN at 10 mg kg^{-1} DOX dose was injected via tail vein of the brain metastases-bearing mice two weeks after tumor inoculation. The metastases-bearing brain was resected 2 h following treatment and transferred to 10% buffered formalin. Texas red-labeled dextran (70 000 MW, Life Technologies, CA) was administered intravenously 15 min prior to euthanasia. Samples were sectioned and stained for nuclei with Hoechst 33342. The fluorescent images of Texas red-dextran (555 nm), DOX (488 nm), and Hoechst 33342 (405 nm) were acquired with Zeiss LSM 700 laser scanning microscopy and overlaid by ImageJ software (National Institutes of Health, Washington, DC, USA).

Evaluation of Tumor-Associated Macrophage Population and Organ Toxicity In Vivo: Three weeks following tumor inoculation, brain metastasis-bearing mice were intravenously injected with the following formulations: 1) saline; 2) iRGD-TPLN; 3) free DOX/MMC (6 mg kg^{-1} DOX dose); 4) DMTPLN (6 mg kg^{-1} DOX dose); 5) iRGD-DMTPLN (6 mg kg^{-1} DOX dose). Organs including brain, liver, lung, kidney, and heart were resected 3 d after treatment and fixed in 10% buffered formalin. Metastases-bearing brains were sectioned and stained with murine anti-F4/80 antibody (Bio-Rad, Hercules, CA, USA) for TAM and murine anti-TMEM119 antibody (Abcam, Toronto, ON, Canada) for microglia.

Fixed liver, lung, kidney, and heart were then examined for toxicity following hematoxylin and eosin (H&E) staining (CFIBCR Histology/Microscope Core Unit, Toronto, ON, Canada). The acute cardiac toxicity was also evaluated by measuring serum cardiac troponin-I (cTnI) level using the mouse cardiac troponin I ELISA kit (Life Diagnostics, Inc. West Chester, PA, USA).

Evaluation of In Vivo Therapeutic Efficacy: When the brain tumor bioluminescence was detectable at about one week after tumor inoculation (recorded as Day 0), the brain metastasis-bearing mice were treated by intravenous injection of the following preparations: 1) saline; 2) iRGD-TPLN; 3) free DOX/MMC (6 mg kg^{-1} DOX dose); 4) DMTPLN (6 mg kg^{-1} DOX dose); 5) iRGD-DMTPLN (6 mg kg^{-1} DOX dose), where the molar ratio of DOX to MMC was maintained at 1: 0.7. 14 d later, the mice received an identical second treatment (recorded as Day 14). This dosing regimen was determined from dose tolerance studies, where free DOX/MMC solution at DOX dose of 6 mg kg^{-1} and 10 mg kg^{-1} (DOX and MMC at fixed molar ratio of 1:0.7) was intravenously injected to brain-metastasis-bearing mice using a two-dose biweekly regimen as previously described.[17b] Since the free solution of DOX/MMC at DOX dose of 10 mg kg^{-1} caused significant body weight loss of ≈20% one week post-treatment (data not shown), DOX dose of 6 mg kg^{-1} was used. Tumor growth was monitored weekly for up to 28 d by bioluminescent imaging using Xenogen imager with 1 min exposure time. The signal intensity of brain metastases was quantified as the sum of all detected photon counts within the ROI. The conditions of the mice (e.g., body weight and fur conditions) were continuously monitored to make decisions regarding their survival time.

Statistical Analysis: All quantitative data are presented as mean ± standard deviation (SD). Student's *t*-test or one-way analysis of variance (ANOVA) followed by Tukey's post-hoc test was performed to determine statistical significance between two or more groups, respectively. One-way repeated ANOVA was used for the changes over time among treatment groups. The log rank test was used to compare treatment groups in the survival study. All statistical tests were done in IBM SPSS Software (Chicago, IL, USA). *p*-values < 0.05 were considered significant.

Supporting Information

Supporting Information is available from the Wiley Online Library or from the author.

Acknowledgements

Conflict of Interest

The authors declare no conflict of interest.

Keywords

blood–brain barrier, brain metastases, multitargeted nanoparticles, triple negative breast cancer, tumor-associated macrophages

[1] A. Diana, E. Franzese, S. Centonze, F. Carlino, C. M. D. Corte, J. Ventriglia, A. Petrillo, F. De Vita, R. Alfano, F. Ciardiello, M. Orditura, *Curr. Oncol. Rep.* **2018**, *20*, 76.

[2] a) N. U. Lin, E. Claus, J. Sohl, A. R. Razzak, A. Arnaout, E. P. Winer, *Cancer* **2008**, *113*, 2638; b) J. Jin, Y. Gao, J. Zhang, L. Wang, B. Wang, J. Cao, Z. Shao, Z. Wang, *BMC Cancer* **2018**, *18*, 446.

[3] a) P. Schmid, S. Adams, H. S. Rugo, A. Schneeweiss, C. H. Barrios, H. Iwata, V. Dieras, R. Hegg, S. A. Im, G. Shaw Wright, V. Henschel, L. Molinero, S. Y. Chui, R. Funke, A. Husain, E. P. Winer, S. Loi, L. A. Emens, I. M. T. Investigators, *N. Engl. J. Med.* **2018**, *319*, 2108; b) D. Arosio, L. Manzoni, C. Corno, P. Perego, *Recent Pat. Anti-Cancer Drug Discovery* **2017**, *12*, 148; c) J. M. Lebert, R. Lester, E. Powell, M. Seal, J. McCarthy, *Curr. Oncol.* **2018**, *25*, S142.

[4] a) H. Hamidi, J. Ivaska, *Nat. Rev. Cancer* **2018**, *18*, 533; b) A. Vogetseder, S. Thies, B. Ingold, P. Roth, M. Weller, P. Schraml, S. L. Goodman, H. Moch, *Int. J. Cancer* **2013**, *133*, 2362; c) J. S. Desgrosellier, D. A. Cheresh, *Nat. Rev. Cancer* **2010**, *10*, 9; d) M. Lorger, J. S. Krueger, M. O'Neal, K. Staflin, B. Felding-Habermann, *Proc. Natl. Acad. Sci. USA* **2009**, *106*, 10666.

[5] R. Stupp, M. E. Hegi, T. Gorlia, S. C. Erridge, J. Perry, Y.-K. Hong, K. D. Aldape, B. Lhermitte, T. Pietsch, D. Grujicic, *Lancet Oncol.* **2014**, *15*, 1100.

[6] a) Y. Zhong, F. Meng, C. Deng, Z. Zhong, *Biomacromolecules* **2014**, *15*, 1955; b) E. Ruoslahti, *Adv. Mater.* **2012**, *24*, 3747; c) F. Danhier, A. Le Breton, V. r. Préat, *Mol. Pharmaceutics* **2012**, *9*, 2961.

[7] a) A. J. Shuhendler, P. Prasad, M. Leung, A. M. Rauth, R. S. DaCosta, X. Y. Wu, *Adv. Healthcare Mater.* **2012**, *1*, 600; b) D. Shan, J. Li, P. Cai, P. Prasad, F. Liu, A. M. Rauth, X. Y. Wu, *Drug Delivery Transl. Res.* **2015**, *5*, 15.

[8] a) A. J. Shuhendler, P. Prasad, R. X. Zhang, M. A. Amini, M. Sun, P. P. Liu, R. G. Bristow, A. M. Rauth, X. Y. Wu, *Mol. Pharmaceutics* **2014**, *11*, 2659; b) A. J. Shuhendler, R. Y. Cheung, J. Manias, A. Connor, A. M. Rauth, X. Y. Wu, *Breast Cancer Res. Treat.* **2010**, *119*, 255; c) A. J. Shuhendler, P. J. O'Brien, A. M. Rauth, X. Y. Wu, *Drug Metab. Drug Interact.* **2007**, *22*, 201; d) T. Zhang, P. Prasad, P. Cai, C. He, D. Shan, A. M. Rauth, X. Y. Wu, *Acta Pharmacol. Sin.* **2017**, *38*, 835.

[9] K. N. Sugahara, T. Teesalu, P. P. Karmali, V. R. Kotamraju, L. Agemy, O. M. Girard, D. Hanahan, R. F. Mattrey, E. Ruoslahti, *Cancer Cell* **2009**, *16*, 510.

[10] a) D. Hanahan, L. M. Coussens, *Cancer Cell* **2012**, *21*, 309; b) M. J. Ernsting, B. Hoang, I. Lohse, E. Undzys, P. Cao, T. Do, B. Gill, M. Pintilie, D. Hedley, S. D. Li, *J. Controlled Release* **2015**, *206*, 122.

[11] a) N. Rippaus, D. Taggart, J. Williams, T. Andreou, H. Wurdak, K. Wronski, M. Lorger, *Oncotarget* **2016**, *7*, 41473; b) D. F. Quail, J. A. Joyce, *Cancer Cell* **2017**, *31*, 326; c) B. Z. Qian, J. W. Pollard, *Cell* **2010**, *141*, 39.

[12] a) X. Zhao, J. Qu, Y. Sun, J. Wang, X. Liu, F. Wang, H. Zhang, W. Wang, X. Ma, X. Gao, S. Zhang, *Oncotarget* **2017**, *8*, 30576; b) M. De Palma, C. E. Lewis, *Cancer Cell* **2013**, *23*, 277; c) S. Q. Qiu, S. J. H. Waaijer, M. C. Zwager, E. G. E. de Vries, B. van der Vegt, C. P. Schroder, *Cancer Treat. Rev.* **2018**, *70*, 178.

[13] a) A. Mantovani, F. Marchesi, A. Malesci, L. Laghi, P. Allavena, *Nat. Rev. Clin. Oncol.* **2017**, *14*, 399; b) F. T. Andon, E. Digifico, A. Maeda, M. Erreni, A. Mantovani, M. J. Alonso, P. Allavena, *Semin. Immunol.* **2017**, *34*, 103; c) K. Binnemars-Postma, G. Storm, J. Prakash, *Int. J. Mol. Sci.* **2017**, *18*.

[14] a) S. Shen, H. J. Li, K. G. Chen, Y. C. Wang, X. Z. Yang, Z. X. Lian, J. Z. Du, J. Wang, *Nano Lett.* **2017**, *17*, 3822; b) P. F. Zhao, W. M. Yin, A. H. Wu, Y. S. Tang, J. Y. Wang, Z. Z. Pan, T. T. Lin, M. Zhang, B. F. Chen, Y. F. Duan, Y. Z. Huang, *Adv. Funct. Mater.* **2017**, *27*; c) M. A. Amini, A. Z. Abbasi, P. Cai, H. Lip, C. R. Gordijo, J. Li, B. Chen, L. Zhang, A. M. Rauth, X. Y. Wu, *J. Natl. Cancer Inst.* **2019**, *111*, 399.

[15] I. J. Fidler, *Semin. Cancer Biol.* **2011**, *21*, 107.

[16] F. Arshad, L. Wang, C. Sy, S. Avraham, H. K. Avraham, *Pathol. Res. Int.* **2010**, *2011*, 920509.

[17] a) C. He, J. Li, P. Cai, T. Ahmed, J. T. Henderson, W. D. Foltz, R. Bendayan, A. M. Rauth, X. Y. Wu, *Adv. Funct. Mater.* **2018**, *28*, 1705668; b) J. Li, P. Cai, A. Shalviri, J. T. Henderson, C. He, W. D. Foltz, P. Prasad, P. M. Brodersen, Y. Chen, R. DaCosta, A. M. Rauth, X. Y. Wu, *ACS Nano* **2014**, *8*, 9925; c) C. He, P. Cai, J. Li, T. Zhang, L. Lin, A. Z. Abbasi, J. T. Henderson, A. M. Rauth, X. Y. Wu, *J. Controlled Release* **2017**, *246*, 98.

[18] a) J. Kreuter, D. Shamenkov, V. Petrov, P. Ramge, K. Cychutek, C. Koch-Brandt, R. Alyautdin, *J. Drug Targeting* **2002**, *10*, 317; b) S. Wagner, A. Zensi, S. L. Wien, S. E. Tschickardt, W. Maier, T. Vogel, F. Worek, C. U. Pietrzik, J. Kreuter, H. von Briesen, *PLoS One* **2012**, *7*, e32568; c) P. Ramge, R. E. Unger, J. B. Oltrogge, D. Zenker, D. Begley, J. Kreuter, H. Von Briesen, *Eur. J. Neurosci.* **2000**, *12*, 1931; d) J. Kreuter, *J. Microencapsulation* **2013**, *30*, 49.

[19] a) J. G. Parvani, M. D. Gujrati, M. A. Mack, W. P. Schiemann, Z. R. Lu, *Cancer Res.* **2015**, *75*, 2316; b) A. L. Allan, R. George, S. A. Vantyghem, M. W. Lee, N. C. Hodgson, C. J. Engel, R. L. Holliday, D. P. Girvan, L. A. Scott, C. O. Postenka, W. Al-Katib, L. W. Stitt, T. Uede, A. F. Chambers, A. B. Tuck, *Am. J. Pathol.* **2006**, *169*, 233; c) T. Meyer, J. F. Marshall, I. R. Hart, *Br. J. Cancer* **1998**, *77*, 530; d) A. Gaultier, G. Simon, S. Niessen, M. Dix, S. Takimoto, B. F. Cravatt 3rd, S. L. Gonias, *J. Proteome Res.* **2010**, *9*, 6689; e) N. D. Staudt, M. Jo, J. Hu, J. M. Bristow, D. P. Pizzo, A. Gaultier, S. R. VandenBerg, S. L. Gonias, *Cancer Res.* **2013**, *73*, 3902; f) R. Covarrubias, A. J. Wilhelm, A. S. Major, *PLoS One* **2014**, *9*, e102236.

[20] a) R. Y. Cheung, A. M. Rauth, P. T. Ronaldson, R. Bendayan, X. Y. Wu, *Eur. J. Pharm. Biopharm.* **2006**, *62*, 321; b) R. X. Zhang, P. Cai, T. Zhang, K. Chen, J. Li, J. Cheng, K. S. Pang, H. A. Adissu, A. M. Rauth, X. Y. Wu, *Nanomedicine* **2016**, *12*, 1279.

[21] R. X. Zhang, H. L. Wong, H. Y. Xue, J. Y. Eoh, X. Y. Wu, *J. Controlled Release* **2016**, *240*, 489.

[22] R. E. Smith, R. MacQuarrie, *Anal. Biochem.* **1978**, *90*, 246.

[23] Y. Zhou, C. He, K. Chen, J. Ni, Y. Cai, X. Guo, X. Y. Wu, *J. Controlled Release* **2016**, *243*, 11.

[24] a) M. Patel, J. Morrow, F. R. Maxfield, D. K. Strickland, S. Greenberg, I. Tabas, *J. Biol. Chem.* **2003**, *278*, 44799; b) B. Taciak, M. Bialasek, A. Braniewska, Z. Sas, P. Sawicka, L. Kiraga, T. Rygiel, M. Krol, *PLoS One* **2018**, *13*, e0198943.

[25] W. Kang, D. Svirskis, V. Sarojini, A. L. McGregor, J. Bevitt, Z. Wu, *Oncotarget* **2017**, *8*, 36614.

[26] J. Ye, X. Xia, W. Dong, H. Hao, L. Meng, Y. Yang, R. Wang, Y. Lyu, Y. Liu, *Int. J. Nanomed.* **2016**, *11*, 4125.

[27] a) A. M. Hamilton, S. Aidoudi-Ahmed, S. Sharma, V. R. Kotamraju, P. J. Foster, K. N. Sugahara, E. Ruoslahti, B. K. Rutt, *J. Mol. Med.* **2015**, *93*, 991; b) K. Wang, X. Zhang, Y. Liu, C. Liu, B. Jiang, Y. Jiang, *Biomaterials* **2014**, *35*, 8735.

[28] X. S. Liu, J. H. Jiang, Y. Ji, J. Q. Lu, R. Chan, H. Meng, *Mol. Syst. Des. Eng.* **2017**, *2*, 370.

[29] R. Noy, J. W. Pollard, *Immunity* **2014**, *41*, 49.

[30] W. Zhou, S. Q. Ke, Z. Huang, W. Flavahan, X. Fang, J. Paul, L. Wu, A. E. Sloan, R. E. McLendon, X. Li, J. N. Rich, S. Bao, *Nat. Cell Biol.* **2015**, *17*, 170.

[31] X. Chen, M. Lowe, T. Herliczek, M. J. Hall, C. Danes, D. A. Lawrence, K. Keyomarsi, *J. Natl. Cancer Inst.* **2000**, *92*, 1999.

[32] K. Chatterjee, J. Zhang, N. Honbo, J. S. Karliner, *Cardiology* **2010**, *115*, 155.

[33] O. J. Arola, A. Saraste, K. Pulkki, M. Kallajoki, M. Parvinen, L.-M. Voipio-Pulkki, *Cancer Res.* **2000**, *60*, 1789.

[34] a) A. Shalviri, G. Raval, P. Prasad, C. Chan, Q. Liu, H. Heerklotz, A. M. Rauth, X. Y. Wu, *Eur. J. Pharm. Biopharm.* **2012**, *82*, 587; b) A. Shalviri, H. K. Chan, G. Raval, M. J. Abdekhodaie, Q. Liu, H. Heerklotz, X. Y. Wu, *Colloids Surf., B* **2013**, *101*, 405.

[35] J. D. Humphries, N. R. Schofield, Z. Mostafavi-Pour, L. J. Green, A. N. Garratt, A. P. Mould, M. J. Humphries, *J. Biol. Chem.* **2005**, *280*, 10234.

[36] a) J. E. Allen, A. S. Patel, V. V. Prabhu, D. T. Dicker, J. M. Sheehan, M. J. Glantz, W. S. El-Deiry, *Cancer Res.* **2014**, *74*, 2385; b) D. P. Kodack, V. Askoxylakis, G. B. Ferraro, D. Fukumura, R. K. Jain, *Cancer Cell* **2015**, *27*, 163.